Elastic properties of a unidirectional SiC_f/Ti composite: Acoustic-resonance measurements and micromechanics predictions

Hirotsugu Ogi[a)]
Graduate School of Engineering Science, Osaka University, Machikaneyama 1-3, Toyonaka, Osaka 560-8531, Japan

Martin L. Dunn
Department of Mechanical Engineering, University of Colorado, Boulder, Colorado 80309

Kazuki Takashima
Precision and Intelligence Laboratory, Tokyo Institute of Technology, Midori-ku, Yokohama, Kanagawa 226-8503, Japan

Hassel Ledbetter
Materials Science and Engineering Laboratory, National Institute of Standards and Technology, Boulder, Colorado 80303

(Received 18 October 1999; accepted for publication 14 December 1999)

Using the mode-selective contactless resonance ultrasound spectroscopy, we measured the complete elastic-stiffness tensor C_{ij} and the corresponding internal-friction tensor Q_{ij}^{-1} of a silicon-carbide fiber unidirectionally reinforced Ti–6Al–4V-matrix composite. This material shows orthorhombic symmetry and possesses nine independent C_{ij} and Q_{ij}^{-1}. We independently excited and detected an unique vibration-mode group among the eight vibration groups of a orthorhombic rectangular parallelepiped. This provides a great advantage in identifying the vibration modes of the observed resonance peaks, whose frequencies yield the C_{ij} by solving an inverse problem. To verify the resultant C_{ij}, we also determined C_{ij} by point-contact resonance ultrasound spectroscopy and pulse-echo methods. Then, using the composite C_{ij}, we inversely calculated the transverse-isotropic fiber elastic stiffnesses with micromechanics theory. With the fiber C_{ij} and the isotropic matrix C_{ij}, we reconstructed the composite C_{ij} as a function of fiber-volume fraction.
 [S0021-8979(00)07206-6]

I. INTRODUCTION

Metal-matrix composites are important materials. Their good mechanical properties, even at elevated temperatures, make them attractive for use in critical components. This study focused on the elastic properties of a silicon-carbide-fiber (SiC_f) unidirectionallly reinforced titanium-alloy composite, which is a candidate material for components of jet engine or aerospace structures because of its high-temperature strength, stiffness, and toughness.[1] First, we measured the elastic stiffnesses C_{ij} and internal friction values Q_{ij}^{-1}. From the manufacturing process, the material shows orthorhombic symmetry and possesses nine independent C_{ij}. Presumably, it also possesses the corresponding nine internal friction Q_{ij}^{-1}. Second, we inversely calculated the fiber C_{ij} with micromechanics theory using the measured composite C_{ij}.

Concerning the elastic-stiffness measurement, we use three methods: electromagnetic acoustic resonance (EMAR), resonance ultrasound spectroscopy (RUS), and the pulse-echo method. The RUS method[2–5] is useful for determining a complete set of C_{ij} of solids. A single-frequency scan provides a large number of mechanical-resonance peaks, which are entered into the inverse calculation to find the most suitable C_{ij}. This method is powerful for a well-posed monocrystal or polycrystal and typically yields C_{ij} within one part in 10^4 or less. However, for a composite material, some obstacles occur; imperfect fiber alignment and heterogeneous phase distribution result in departure from ideal macroscopic symmetry. These characteristics may cause spectrum split, resonance-peak broadening, and nonsymmetrical resonance peaks. In this case, the mode identification (exact correspondence between the measured and calculated frequencies) is not straightforward, and the inverse calculation easily converges to a false minimum. Note that the resultant C_{ij} from incorrect mode identification have no physical meaning.

In previous studies,[6,7] we established the contactless, mode-selective RUS method. We call this method EMAR.

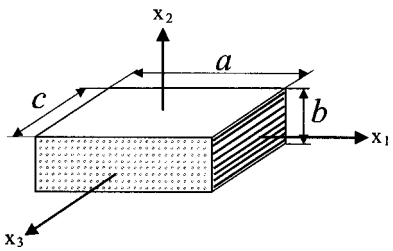

FIG. 1. Unidirectionally fiber-reinforced-composite specimen and coordinate system.

[a)]Also at Materials Science and Engineering Laboratory, National Institute of Standards and Technology, Boulder, Colorado 80303; electronic mail: ogi@me.es.osaka-u.ac.jp

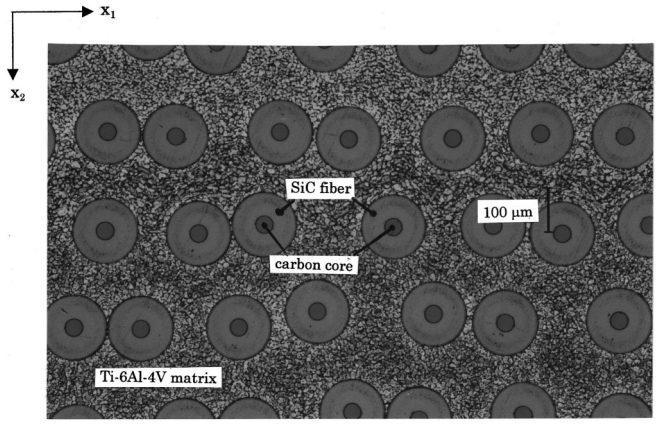

FIG. 2. Microstructure of the composite seen along the x_3 axis.

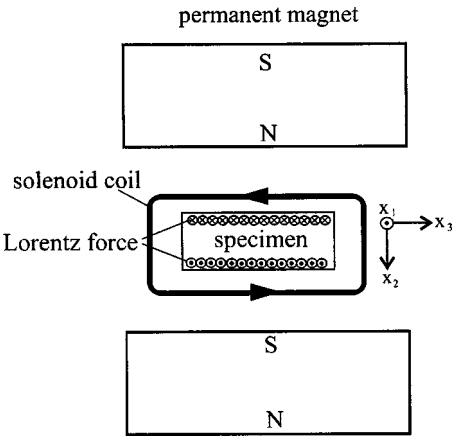

FIG. 3. EMAR measurement setup for B_{1g} vibration group.

Using the Lorentz-force coupling, we selectively and independently generated and detected one vibration group among the eight vibration groups of rectangular parallelepipeds. This is a great advantage for mode identification because only one vibration group appears and no mode overlapping occurs. We applied this method to a copper monocrystal (cubic)[6] and SiC_f/Ti-alloy crossply composite (tetragonal),[7] and obtained successful results. In this study, we applied this method to a lower symmetry case (orthorhombic) and compared the results with the usual RUS and the pulse-echo methods. The acoustically contactless configuration of EMAR is ideal for measuring internal friction. We measured the internal-friction tensor Q_{ij}^{-1} by the free-decay method with EMAR.

For theoretical calculations, we used the Mori–Tanaka mean-field theory.[8] With the assumption of transverse symmetry for the SiC fiber and isotropic symmetry for the matrix, we inversely calculated the effective fiber elastic stiffnesses. Then, we reconstructed the composite C_{ij} as a function of volume fraction.

II. MATERIAL

The composite was a Ti–6Al–4V alloy reinforced with continuous SCS-6SiC fibers. Figure 1 shows the schematic of the material and the coordinate system used in the present study. Figure 2 shows microstructure observed along the x_3 axis. The fiber consists of a carbon core surrounded by SiC. The fiber diameter is 140 μm and the fiber volume fraction is 0.35. The material was fabricated by a foil-fiber-foil technique (8 ply) at 900 °C with 65 MPa hydrostatic compression. We prepared three rectangular-parallelepiped specimens (specimens A, B, and C) with dimensions given in Table I. We measured mass density by the Archimedes method, which also appears in Table I. This material exhibits orthorhombic symmetry with nine independent C_{ij}.

TABLE I. Specimen dimensions and mass density.

	a (mm)	b (mm)	c (mm)	ρ (kg/m^3)
Specimen A	4.943	1.745	3.979	3870
Specimen B	3.986	1.815	3.023	3886
Specimen C	4.484	1.742	3.967	3879

$$[C_{ij}]=\begin{bmatrix} C_{11} & C_{12} & C_{13} & 0 & 0 & 0 \\ C_{12} & C_{22} & C_{23} & 0 & 0 & 0 \\ C_{13} & C_{23} & C_{33} & 0 & 0 & 0 \\ 0 & 0 & 0 & C_{44} & 0 & 0 \\ 0 & 0 & 0 & 0 & C_{55} & 0 \\ 0 & 0 & 0 & 0 & 0 & C_{66} \end{bmatrix}. \quad (1)$$

III. MEASUREMENTS

The EMAR-measurement setup is the same as that developed in the previous studies.[6,7] The specimen was inserted in a solenoidal coil located between two permanent-magnet blocks. The solenoidal coil is driven with high-power rf bursts, which cause eddy currents near the surface region of the specimen. Eddy currents interact with the static magnetic field from the permanent magnets and generate Lorentz forces. The Lorentz force vibrates with the same frequency as the driving bursts, being sources of mechanical vibration. The same coil receives the vibration through the reversed-Lorentz-force mechanism. The received signals are fed to superheterodyne phase detectors, and the amplitude spectrum at the operating frequency is determined. A single-frequency scan provides many resonance peaks, and the resonance frequencies are determined by Lorentzian-function fitting.

The free vibrations of a rectangular parallele piped with orthorhombic or higher symmetry fall into eight groups depending on the deformation symmetry.[2] Because the Lorentz-force direction is determined by the vector product of the magnetic field and eddy currents, we can control the deformation symmetry and select a vibration group by changing the geometrical configuration between the static field and the solenoidal coil. For example, in Fig. 3, the magnetic field is applied along the x_2 axis and the Lorentz-forces work on the x_1-x_3 faces along the x_1 axis. The Lorentz forces cause the x_1-component displacement u_1. This displacement can be detected most effectively by the same coil through the reversed-Lorentz-force mechanism when u_1 is an odd function about x_2 and an even function about x_1

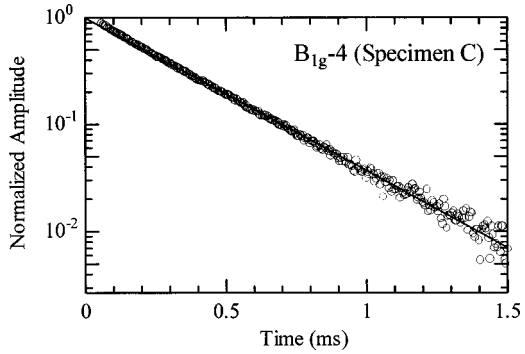

FIG. 4. Free decay of the amplitude after excitation. Open circles denote measurements, and solid line denotes the fitted exponential function.

and x_3. Among the eight groups of free vibration, only the B_{1g} vibration group (torsional vibration about x_3 axis) satisfies this condition.[9] Thus, only B_{1g} vibration modes are generated and detected with this configuration. In this study, we independently excited and detected B_{1g}, B_{3g} (torsional vibration about x_1 axis), and A_g (breathing vibration) groups. The EMAR configurations for B_{3g} and A_g groups appear in Refs. 6 and 7. Details of RUS and pulse-echo measurements are described in Ref. 5.

For internal friction, we measured the amplitude decay after an excitation with a burst signal.[10] The amplitude free-decay curve provides the internal friction at the resonance frequency. Figure 4 shows the result of the measured amplitude decay and the fitted exponential function. Internal frictions for all resonance modes were used to reduce the internal-friction tensor Q_{ij}^{-1}, which enable us to calculate the internal friction of any unmeasurable oscillation mode.

IV. MICROMECHANICS MODELING

We briefly describe a micromechanics model used to estimate the effective stiffness of the composite in terms of the fiber and matrix elastic stiffnesses and the fiber volume fraction. Our intent is to use this model to derive the unknown effective SiC fiber elastic stiffness from the measured composite stiffness and the known matrix C_{ij}. We use the term *effective* to describe the fiber stiffness because the fibers themselves have a composite structure (see Fig. 2) consisting of an SiC annulus surrounding a carbon core. Furthermore, the thin interface region between the SiC and Ti matrix also affects the effective SiC fiber elastic stiffness.

For the analysis, we considered the unidirectional SiC/Ti composite to be a two-phase composite consisting of the matrix (phase 0) and the aligned fibers (phase 1). We introduced a coordinate system where x_3 is parallel to the unidirectional fibers. We assumed transverse-isotropic symmetry for the fiber and isotropic symmetry for the matrix. Also, we assumed transverse-isotropic symmetry for the resultant composite C_{ij} because of simplicity of calculation. (In the general development, the composite will exhibit lower symmetry, but as will be shown later, the measured composite C_{ij} showed nearly transverse-isotropic symmetry with a few percent error.) The effective elastic stiffness of the two-phase

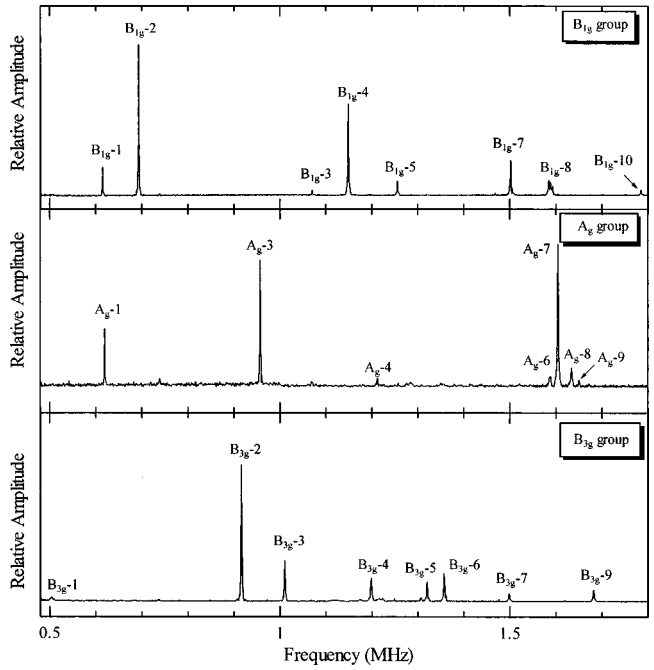

FIG. 5. EMAR resonance spectra of B_{1g} vibration group, A_g vibration group, and B_{3g} vibration group.

composite **C** can be expressed in terms of strain concentration factors as[11,12]

$$\mathbf{C}=c_0\mathbf{C}_0\mathbf{A}_0+c_1\mathbf{C}_1\mathbf{A}_1=\mathbf{C}_0+c_1(\mathbf{C}_1-\mathbf{C}_0)\mathbf{A}_1. \tag{2}$$

Here, $\mathbf{C}_i$ and c_i are the elastic stiffness tensor and the volume fraction of the ith phase, and $\mathbf{A}_i$ are the strain concentration factors for the ith phase. Bold symbols are used for tensorial quantities. Physically, the strain concentration factors relate the average strain in the ith phase to the uniform strain that would be developed in a homogeneous material if it were subjected to displacement boundary conditions. In other words, $\boldsymbol{\epsilon}_i=\mathbf{A}_i\boldsymbol{\epsilon}^0(i=0,1)$, where $\boldsymbol{\epsilon}^0$ is the uniform strain consistent with the applied displacements. The second term in the right-hand side of Eq. (2) comes from the identities $c_0+c_1=1$ and $c_0\mathbf{A}_0+c_1\mathbf{A}_1=I$. As is apparent from Eq. (2), the key to predicting the effective stiffness of the composite is estimating the concentration factors $\mathbf{A}_i$. Here, we use the Mori–Tanaka mean-field theory[8] to estimate $\mathbf{A}_i$. The physical interpretation of the theory is that, when subjected to uniform stress boundary conditions, the average stress in each fiber is equal to the average stress in a single fiber embedded in an infinite matrix subjected to a uniform far-field stress equal to (as-yet unknown) average stress in the composite. Mathematically, this assumption can be written as

$$\begin{aligned}&\mathbf{A}_i=\mathbf{A}_{Di}^{-1}[c_0\mathbf{I}+c_1\mathbf{A}_{D1}],\\&\mathbf{A}_{Di}=\mathbf{I}+\mathbf{S}\mathbf{C}_0^{-1}(\mathbf{C}_i-\mathbf{C}_0).\end{aligned} \tag{3}$$

Hence, $\mathbf{A}_{Di}$ is the concentration factor for a single fiber of phase i embedded in an infinite matrix subjected to uniform far-field stress or strain boundary conditions and is called the dilute concentration factor. It is easily determined analytically by using Eshelby's equivalent inclusion method.[13–15]

The effect of the fiber shape is contained in the Eshelby tensor **S**, which is a function of the fiber shape, and Poisson's ratio of the isotropic matrix ν. For the fiber shape considered here, continuous circular cylinders, the nonzero components of **S** are remarkably simple and are tabulated in Mura's monograph,[14] along with results for other inclusion shapes.

Our intent was to use this model inversely to find the effective-elastic-stiffness tensor of the fibers. Some model calculations that used isotropic elastic moduli for the SiC fibers have been reported in the literature,[16,17] but as we shall show, the assumption of isotropic fibers is inconsistent with the measured composite stiffness (and, of course, with the annular fiber morphology). Our micromechanics estimates then yielded explicit expressions for the five independent elastic stiffness components of the composite C_{ij} in the form

$$C_{ij}=C_{ij}(C_{0_{11}},C_{0_{44}},C_{1_{11}},C_{1_{13}},C_{1_{33}},C_{1_{44}},C_{1_{66}},c_1). \quad (4)$$

Thus, Eq. (4) represents five equations that connect the five composite C_{ij} to the five fiber C_{1ij}, the two matrix C_{0ij}, and the fiber volume fraction c_1. From our measurements, we reduced the nine composite C_{ij} to five C_{ij} by assuming transverse isotropy of the composite. (We used the measured C_{12}, C_{11}, and C_{66} and formed an error function with the calculated C_{12}, C_{11}, and C_{66}, which averages the measured C_{12}, C_{11}, and C_{66}. For the other C_{ij}, we simply averaged the orthorhombic C_{ij}.) For the matrix, we used $C_{011}=160.6\,\text{GPa}$ and $C_{044}=42.0\,\text{GPa}$.[18] The fiber volume fraction is $c_1=0.35$. We used these values with the five Eqs. (4) to inversely compute the five fiber C_{1ij}.

V. RESULTS AND DISCUSSION

A. Elastic stiffnesses

Figure 5 shows the resonance spectra measured by EMAR for specimen *A*. Different EMAR configurations led to a different spectrum pattern, as expected. According to the mode-selection principle, we identified the resonance modes and made the inverse calculation developed in the previous study[5] to determine the nine independent elastic stiffnesses. Table II compares the measured and calculated resonance

TABLE II. Measured (f_{EMAR}) and calculated (f_{calc}) resonance frequencies with EMAR for specimen B. Mode notation follows Mochizuki (see Ref. 9). The average difference of $f_{\text{EMAR}}-f_{\text{calc}}$ was 0.4%.

Mode	f_{EMAR} (MHz)	f_{calc} (MHz)	diff. (%)
$B_{1g}-1$	0.633727	0.639325	0.88
$B_{1g}-2$	0.761856	0.767144	0.69
$B_{1g}-3$	1.112402	1.11038	−0.18
$B_{1g}-4$	1.189886	1.179541	−0.87
$B_{1g}-5$	1.286432	1.282397	−0.31
$B_{1g}-6$	1.427158	1.429458	0.16
$B_{1g}-7$	⋯	1.604195	⋯
$B_{1g}-8$	1.638866	1.64696	0.49
$B_{1g}-9$	⋯	1.760986	⋯
$B_{1g}-10$	⋯	1.887708	⋯
$B_{1g}-11$	⋯	1.925395	⋯
$B_{1g}-12$	1.93206	1.929845	−0.11
A_g-1	0.674023	0.671491	−0.38
A_g-2	⋯	0.798739	⋯
A_g-3	0.958798	0.954882	−0.41
A_g-4	⋯	1.244947	⋯
A_g-5	1.490086	1.486785	−0.22
A_g-6	1.594972	1.60392	0.56
A_g-7	⋯	1.66483	⋯
A_g-8	1.673748	1.672069	−0.1
A_g-9	⋯	1.67851	⋯
A_g-10	1.83982	1.828107	−0.64
A_g-11	1.85286	1.864525	0.63
A_g-12	1.938973	1.944108	0.26
A_g-13	2.007576	2.010206	0.13
$B_{3g}-1$	0.551647	0.551056	−0.11
$B_{3g}-2$	0.916413	0.918502	0.23
$B_{3g}-3$	1.052841	1.057635	0.46
$B_{3g}-4$	1.264239	1.263364	−0.07
$B_{3g}-5$	1.317111	1.309443	−0.58
$B_{3g}-6$	1.398568	1.393513	−0.36
$B_{3g}-7$	⋯	1.552009	⋯
$B_{3g}-8$	⋯	1.650926	⋯
$B_{3g}-9$	1.772487	1.781171	0.49
$B_{3g}-10$	1.996798	1.999062	0.11

TABLE III. Composite elastic stiffnesses (GPa) measured by the EMAR, RUS, and pulse-echo (PE) methods; fiber elastic stiffnesses (GPa) determined by the micromechanics theory; and composite internal friction measured by EMAR.

	Specimen A			Specimen B			Specimen C					
	EMAR	RUS	PE	EMAR	RUS	PE	EMAR	RUS	PE	Average[a]	Fiber moduli[b]	Q_{ij}^{-1} (10^{-4})
C_{11}	190.1	190.6	⋯	191.1	189.4	⋯	190.3	189.6	⋯	190.2	278.9	3.14
C_{22}	193.2	190.7	192.9	190.0	190.5	191.9	190.8	190.6	190.7	191.0	278.9	6.90
C_{33}	258.4	258.6	⋯	243.8	244.8	⋯	246.3	246.7	⋯	249.8	418.1	3.54
C_{44}	56.62	55.33	58.7	55.97	54.18	56.13	56.62	56.86	57.06	55.93	93.1	10.8
C_{55}	53.54	57.71	⋯	51.23	55.62	⋯	50.48	55.96	⋯	54.09	93.1	11.7
C_{66}	55.23	55.52	54.1	53.83	54.30	53.77	53.87	54.16	54.85	54.49	109.5	6.78
C_{12}	75.83	79.83	⋯	69.90	75.31	⋯	76.76	75.82	⋯	75.58	59.0	⋯
C_{13}	70.45	69.99	⋯	73.53	68.18	⋯	71.75	69.96	⋯	70.29	50.1	⋯
C_{23}	73.48	76.19	⋯	61.63	63.10	⋯	65.51	65.53	⋯	67.57	50.1	⋯
E_1	152.7	150.9	⋯	153.8	151.3	⋯	150.2	150.8	⋯	151.6	262.6	5.05
E_2	154.1	147.8	⋯	158.8	154.7	⋯	153.7	153.9	⋯	153.8	262.6	13.2
E_3	219.7	218.9	⋯	208.2	212.2	⋯	210.8	212.1	⋯	213.7	403.2	4.35
B	120.1	121.3	⋯	115.0	115.3	⋯	117.3	116.6	⋯	117.6	143.8	1.91

[a]EMAR-RUS average.

[b]Fiber-longitudinal direction is along the x_3 axis.

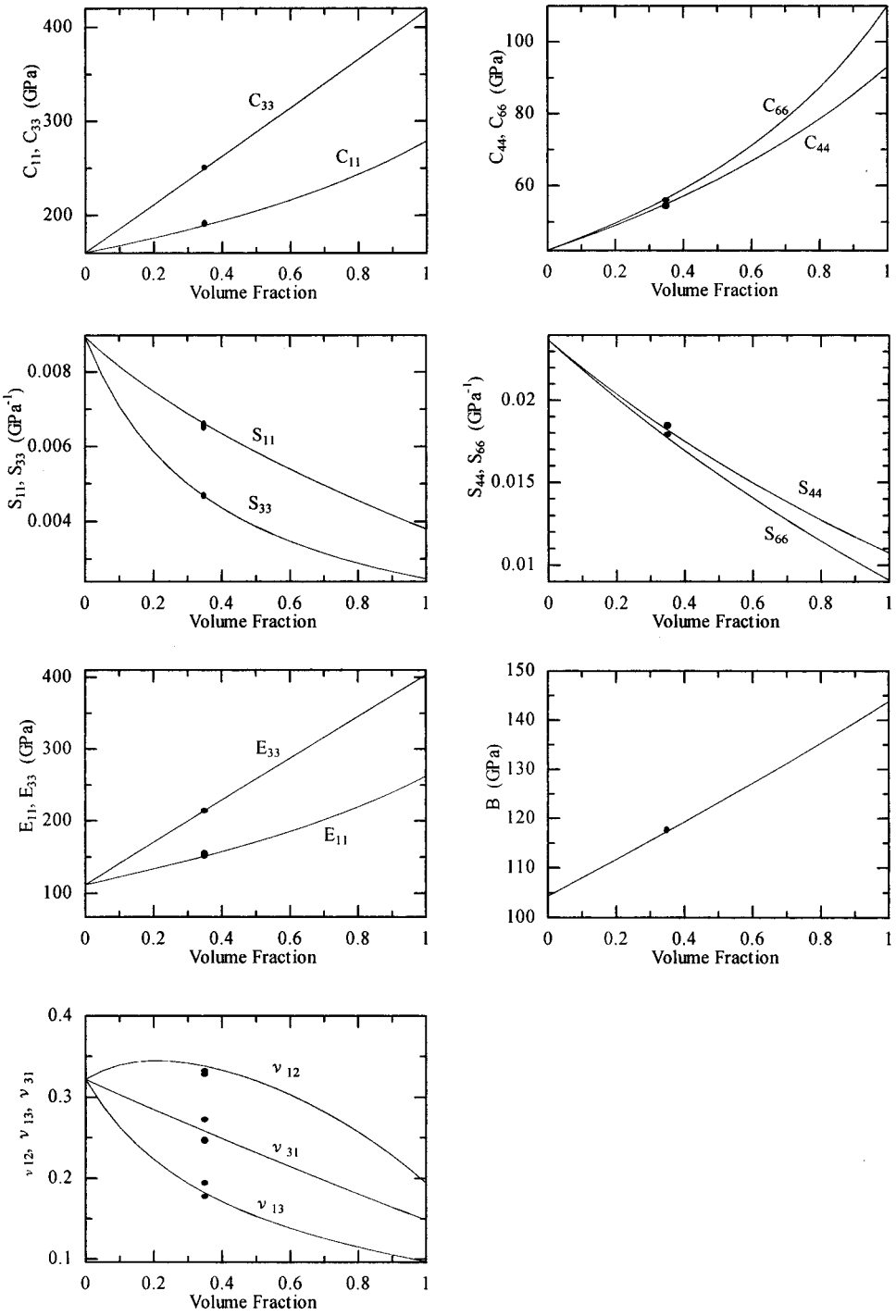

FIG. 6. Composite elastic properties reconstructed using the micromechanics model. Solid circles are measurements.

frequencies for specimen B. For almost all modes, they agreed within 1%. The typical rms error was 0.5%.

We also applied the RUS method. The RUS spectra showed a better signal-to-noise ratio than the EMAR spectra, but the subsequent inverse calculations were very sensitive to the initial estimates of C_{ij} and easily converged to different (false) minima. However, because we used the elastic stiffnesses determined by EMAR as the initial set for the RUS-inverse calculation, the resultant C_{ij} were consistent with EMAR and pulse-echo C_{ij}. The rms difference between measured and calculated frequencies was comparable with that in the EMAR case.

For pulse-echo measurements, we used longitudinal wave and two shear waves polarized in the x_1 and x_3 directions. All ultrasonic waves propagated in the x_2 direction. They provide C_{22}, C_{66}, and C_{44}. The pulse-echo method applied to other propagation directions was unsuccessful because the surface areas were too small.

Table III presents the elastic stiffnesses determined by the three methods. The EMAR and RUS methods gave close C_{ij}, within a few percent difference, except for C_{55}: the RUS C_{55} was about 8% larger than the EMAR C_{55}. At present, this remains unclear. The EMAR and pulse-echo methods showed the same trend of C_{44} larger than C_{66},

which is expected from the fiber alignment. This was not evident with the RUS method, although agreement of the RUS C_{ij} with the pulse-echo C_{ij} was still good. The EMAR measurement is based on the correct mode identification, but it includes fewer resonance peaks. The RUS measurement includes more resonance peaks, but mode identification is unclear, especially at higher modes because the peaks overlap. Therefore, we consider that averaging the elastic stiffnesses obtained by the EMAR and RUS methods provides the most reliable answer; these averages are shown in Table III.

B. Prediction of composite elastic stiffnesses

The measurement results $C_{11}\cong C_{22}$, $C_{44}\cong C_{66}$, and $C_{13}\cong C_{23}$ suggest that the composite has nearly tetragonal symmetry, which is understandable from its manufacturing procedure (foil-fiber-foil technique). For transverse isotropy, the additional requirement is $C_{66}=(C_{11}-C_{12})/2$. This was observed with 5%. As a result, in determining the fiber C_{ij}, we assumed transverse-isotropic symmetry for the composite, which is needed to use Eq. (4) directly; these values are given in Table III. This is the complete set of effective elastic stiffnesses for the SCS-6 SiC fibers. Previously, only axial Young's modulus has been reported; it ranged from 400 to 428 GPa,[19,20] consistent with our inferred value of 403 GPa. Note that we tried to determine the fiber elastic stiffnesses by assuming that they were isotropic and by using the same approach, but we were unsuccessful. This means that no possible set of isotropic fiber C_{ij} can explain the measured composite C_{ij}.

Once we obtain the complete sets of the fiber elastic stiffnesses and the matrix stiffnesses, we can reconstruct the composite stiffness as a function of fiber-volume fraction by using Eq. (2). In Fig. 6, we show the changes in composite elastic properties that are important for engineering purposes.

C. Internal friction

We show the three-specimen averaged internal-friction tensor components Q_{ij}^{-1} in Table III. Possible factors contributing to internal friction in the frequency range used here are the dislocation damping in the matrix and energy loss at the imperfectly bonded fiber-matrix and interlayer boundaries. The bulk-modulus internal friction was the smallest value, which is understandable because dislocation mobility is lower during breathing-mode vibration.[6] An interesting observation is the larger internal friction for the wave modes propagating in the x_2 direction; that is, Q_{22}^{-1} is larger than Q_{11}^{-1} and Q_{33}^{-1}; Q_{44}^{-1} and Q_{55}^{-1} is larger than Q_{66}^{-1}; and Q_{E2}^{-1} is larger than Q_{E1}^{-1} and Q_{E3}^{-1}. This trend is the same as that observed for a similar SiC/Ti crossply composite[7] and suggests an energy loss at the imperfect bonding boundaries between ply layers.

VI. CONCLUSIONS

(1) We determined the complete set of elastic stiffnesses of a unidirectional SiC_f/Ti alloy composite using three methods: electromagnetic acoustic resonance (EMAR), resonance ultrasound spectroscopy (RUS), and pulse echo. In EMAR, we controlled the vibration mode by changing the geometrical configuration of the coil and static field, which is an important advantage in mode identification.

(2) Using the C_{ij} determined by EMAR for the initial guess of the iteration analysis in RUS led to successful inverse-calculation convergence.

(3) Assuming transverse isotropy, we calculated the complete set of the effective SiC fiber elastic stiffnesses using the measured composite C_{ij} and matrix C_{ij} with a micromechanics model. The calculated Young's modulus along the fiber direction agreed with previously reported values. A complete set of the SiC fiber C_{ij} is first reported here.

(4) We applied the micromechanics model to predict the composite C_{ij} as a function of fiber-volume fraction.

(5) We determined the internal-friction tensor Q_{ij}^{-1} by a free-decay method with EMAR. The Q_{ij}^{-1} of wave modes propagating in the x_2 direction were larger than those of other modes, suggesting imperfect bonding between ply layers. Thus, the measurement of the internal-friction tensor indicates the quality of those interfaces.

ACKNOWLEDGMENTS

Gratefully, the authors acknowledge Sudook Kim's (NIST) effort on the pulse-echo measurements. Professor P. Bowen (The University of Birmingham) provided them with the material. C. McCowan (NIST) produced the micrographs.

[1] J. Wadsworth and F. H. Froes, JOM **41**, 12 (1989).
[2] I. Ohno, J. Phys. Earth **24**, 355 (1976).
[3] J. Maynard, Phys. Today **49**, 26 (1996).
[4] A. Migliori and J. Sarrao, *Resonant Ultrasound Spectroscopy* (Wiley, New York, 1997).
[5] H. Ledbetter, C. Fortunko, and P. Heyliger, J. Appl. Phys. **78**, 1542 (1995).
[6] H. Ogi, H. Ledbetter, S. Kim, and M. Hirao, J. Acoust. Soc. Am. **106**, 660 (1999).
[7] H. Ogi, K. Takashima, H. Ledbetter, M. L. Dunn, G. Shimoike, M. Hirao, and P. Bowen, Acta Mater. **47**, 2787 (1999).
[8] T. Mori and K. Tanaka, Acta Metall. **21**, 571 (1973).
[9] E. Mochizuki, J. Phys. Earth **35**, 159 (1987).
[10] H. Ogi, M. Hirao, and T. Honda, J. Acoust. Soc. Am. **98**, 458 (1995).
[11] R. Hill, J. Mech. Phys. Solids **13**, 213 (1965).
[12] G. J. Dvorak, in *Metal Matrix Composites, Mechanisms and Properties*, edited by R. K. Everett and R. J. Arsenault (Academic, Boston, 1991), Vol. 2, pp. 1–77.
[13] J. D. Eshelby, Proc. R. Soc. London, Ser. A **241**, 376 (1957).
[14] T. Mura, *Micromechanics of Defects in Solids*, 2nd ed. (Martinus Nijhoff, 1987).
[15] S. Nemat-Nasser and M. Hori, *Micromechanics: Overall Properties of Heterogeneous Materials*, 2nd ed. (Elsevier, New York, 1999).
[16] J. Y. Li, Int. J. Solids Struct. (in press).
[17] G. J. Dvorak, T. Chen, and J. Teply, Compos. Sci. Technol. **43**, 347 (1992).
[18] E. Naimon, W. Weston, and H. Ledbetter, Cryogenics **14**, 246 (1974).
[19] S. K. Mital, C. C. Chamis, and P. K. Gotsis, Compos. Sci. Technol. **50**, 59 (1994).
[20] G. T. Ward, D. J. Herrmann, and B. M. Hillberry, J. Compos. Technol. Res. **17**, 205 (1995).